Forming of thin-walled AA6061-T4 tubular joint by elastomeric bulging: experiment and computation

Jingchao Yang [1,2] · Heng Li [1,2] · Dan Huang [3] · Guangjun Li [3] · Sheng Yuan [3]

Abstract

Tubular joint forming by elastomeric bulging (EB) is a feasible way to connect aluminum alloy tubes to high-strength sleeve fittings. It is critical to fully and deeply understand the deformation-induced sealing performance of tubular joints for precise manufacturing of high performance tubular joints. In this paper, thin-walled AA6061-T4 tubular joints fabricated by EB was investigated experimentally and numerically. Firstly, the anisotropic AA6061-T4 tube, the polyurethane elastomer (PUE) tube with hyperelasticity and the 15-5PH stainless steel (SS) sleeve fitting were characterized and modeled. Compared with the explicit algorithm, the implicit axisymmetric finite element (FE) models of the whole joining process, including EB forming and springback, were established. The influence of the groove structure of the sleeve fitting on the shearing-related pull-out strength and sealing-related bonding strength was discussed, and then the reasonable sleeve fitting's structure with two grooves was obtained. Thus, the accurate ranges of extrusion pressure and tube bulging heights were derived for precise control of forming quality. Finally, the experimental set-up and forming dies for EB joining tests were established, and the reliability of these parameters determined by the FE model was verified experimentally. It is concluded that the forming quality of this tubular joint can be controlled precisely based on FE modeling of whole joining process, and thin-walled AA6061-T4 tubular joint fabricated by EB has a reliable seal performance.

1 Introduction

Tubular joining fittings are widely applied in many industries such as aviation, aerospace, shipbuilding, automobile, power system, and petrochemical engineering. With continuous increasing of the requirements of lightweight, robust pressure resistance, high reliability, and green manufacture, traditional joining technologies such as welding, brazing, and adhesive bonding present some limitations for manufacturing these tubular joining fittings. However, joining by plastic deformation may present great potential and efficiency to satisfy the above high performance demands for these tubular joining components [1]. Especially, tubular joint forming by plastic deformation is promising in aviation pipeline system. It is generally known that tubular components are spread all over a whole aircraft with the features of large amount and compact structure. For instance, there are thousands of ducts in an aeroengine. These ducts are similar to the blood vessels of the human body and are the most important lifelines on the plane [2]. On one hand, they transfer various media to the engine, the landing gear and the cockpit, etc., meeting the requirements of hydraulic, fuel, environmental control, fire extinguishing, oxygen supply, and pneumatics systems. On the other hand, they are assembled on the aircraft's overall frame as a structure to increase the overall stiffness and strength of the aircraft. Not only does the exterior of these tubular components withstand high and low temperature and high frequency vibration, but the interior also withstands the pulsating impact of the fluid medium, so that their working conditions are very harsh. Therefore, reliable connection

✉ Heng Li
liheng@nwpu.edu.cn

1   State Key Laboratory of Solidification Processing, School of Materials Science and Engineering, Northwestern Polytechnical University, Xi'an 710072, China

2   Yantze River Delta Research institute of NPU, Taicang, China

3   Chengdu Aircraft Industry (Group) Corporation Ltd., Chengdu 610092, China

between the tubes is particularly critical for the whole pipeline systems in aircrafts. Therefore, as key and universal aviation parts for reliable connection, tubular joints require more excellent performances such as light weight, robust pressure resistance, long life and high reliability.

At present, there are two kinds of joining methods for forming tubular joints in aviation pipeline systems, including permanent couplings and separable end fittings [3]. Permanent couplings are used to permanently join hydraulic and pneumatic tubing, but they cannot be disassembled. By contrast, separable end fittings are more versatile, and they can be disassembled for maintenance and replacement. These two kinds of tubular joints are fabricated by many kinds of materials applied in different aviation pipeline systems, including Ti-based alloys [4, 5], Ni-based alloys [6] and Al-based alloys [7]. Aluminum alloy (AA) tubular joints fabricated by elastomeric bulging (EB) belongs to a kind of separable end fittings, also known as a flareless joining type This joint consists of an AA tube and a stainless steel (SS) sleeve fitting. It has better corrosion resistance and anti-vibration performance. However, its sealing performance is unstable. Therefore, it is urgent to investigate the tubular joint forming by EB for finding out the deformation-based sealing mechanism, so as to achieve precise control of forming quality.

In views of the deformation-based joining method, there have been some important investigations. Mori et al. [8] classified joining by plastic deformation as metallurgical joining and mechanical joining, and further introduced joining mechanisms of interference-fit and form-fit joints by means of forming. Based on this study, the joining method in this presentation is with features of interference-fit and form-fit. Groche et al. [9] systematically clarified two joining principles of mechanical joints by forming: form-closed joint and force-closed joint. Referring to the above joining mechanisms, many joining methods for tubular components have been developed. Henriksen et al. [10] investigated a way of joining by bulging using a rigid die with ridges for connecting the pipe and the flange with grooves. Przybylski et al. [11] proposed a joining method by rolling to manufacture a joint for light tubular structures. They indicated that the joint with trapezoid dentils presented a higher disconnecting force compared with cylindrical ones. Weddeling et al. [12], by means of non-destructive testing, investigated the influence of groove structure of form-fit joint on pull-out strength. In order to exclude the effect of interference-fit connection on the pull-out strength, this form-fit joint was manufactured by electromagnetic forming to force the aluminum alloy tube material into the grooves of the same material. Gies et al. [13] investigated form-fit joining by die-less hydroforming and predicted analytically the inner bulging pressure for filling the tube material into the circular circumferential grooves. Additionally, there are also some innovative ways for tubular joining application based on rotary swaging [14, 15], sheet-bulk forming [16] and compression instability [17], etc. Zhang et al. [18] investigated a crimped joint of coper and

aluminum tubes at the overlapping part of tube ends by means of rotary swaging. Alves et al. [19] proposed a joining method on the basis of sheet-bulk forming. This joining process is to form a lap joint of tube and plate by compressing the thinned tube wall. Furthermore, Alves et al. [20] updated and optimized the above joining process by overcoming the esthetic and dimensional limitation and breaking through the restriction under small applied loading. Taking advantage of plastic instability, Alves et al. [21] investigated a tube/tube joining process by their ends to a form tubular butt joint; Yu et al. [22] estimated the formability of this tubular butt joint; Alves et al. [23] also proposed another tube joining way by internal mechanical locking.

In the joining process of this presentation, polyurethane elastomer (PUE) material, as a bulging medium, is a significant factor affecting the forming quality [24]. Therefore, it is essential to get better fundamental knowledge about rubber forming. Girard et al. [25] developed an axisymmetric model of bulging of copper tubes using a urethane rod as bulging medium based on the LS-DYNA finite element (FE) analysis code and verified the model by comparing with the bulge height and thickness distribution of experiments. Ramezani et al. [26] investigated the frictional behavior in the rubber pad forming by means of numerical method. Koubaa et al. [27] studied flexible bulge forming of aluminum alloy sheet metal by using rubber as a medium and predicted the forming capability with the aid of FE simulation. Belhassen et al. [28] considered the anisotropic behavior of aluminum alloy tube and simulated the compression beading process of the tube with rubber via Abaqus/Explicit.

Taking into account the above research, we found that most papers only consider the connection strength of the interference-fit and form-fit tubular joints, while few papers study the deformation-induced sealing performance, which is significant for tubular fittings in aviation pipeline systems. It can be also found that the mechanical properties of PUE are seldom characterized accurately in sheet metal forming process. In this paper, to achieve better deformation-induced sealing performance of tubular joints, we combine FE simulation and experimental verification to investigate thin-walled AA 6061-T4 tubular joint forming by EB. The details are as follows: (1) The AA6061-T4 tube considering anisotropy, the PUE tube with hyperelasticity, and the 15-5PH SS sleeve fitting will be all characterized and modeled for subsequent FE modeling of EB joining process; (2) Based on the above three material models, the axisymmetric implicit FE models of the whole joining process, including loading and unloading, will be established; (3) Reasonable groove structures of sleeve fittings will be designed and analyzed, and feasible ranges of extrusion forming pressure and tube bulging heights will be obtained to achieve precise control of forming quality of the tubular joints; (4) The experimental set-up and forming dies for EB joining tests will be established, and the reliability of these parameters determined by the FE model will be verified by the EB joining tests and the destructive cutting tests.

2 Experimental background

2.1 Joining mechanism

Figure 1 briefly describes an integrated assembly for joining a couple of tubular components. It can be found that this tubular joining component uses a typical detachable way for connecting two tubular separable end fittings. Figure 2 shows the process of tube end forming by EB to fabricate a tubular joint. As can be seen from Fig. 2, EB is a typical plastic forming process: (i) axially extruding the PUE tube to generate internal pressure; (ii) bulging the AA6061-T4 tube and squeezing the tube into the grooves of 15-5PH SS sleeve fitting. After the forming process, the springback simultaneously occurs in the AA tube and the SS sleeve fitting. Due to different elastic moduli of the two parts, an interference pressure between them is generated, and it makes the outer surface of the AA tube closely bond on the inner surface of the sleeve fitting to resist the working pressure inside the AA tube, and thus preventing the leakage. And the undercuts are formed at the sharp edges of the sleeve fitting's grooves to resist the axial disconnecting force. According to the review [8], this joining way is a combination of interference-fit and form-fit.

2.2 Materials characterization

2.2.1 AA 6061-T4 tube

The geometry and dimensions of the AA tube are 20 mm outside diameter × 1 mm wall. For describing the deformation feature of the tube, the tensile test of full-size tubular sections was conducted. Figure 3 illustrates the specimen schematic representation, and it also shows the true stress-strain curve of breaking and the one of stretching to 15% strain where the tube was in the uniform plastic deformation stage. Based on the experimental result, the Lankford coefficient r, i.e., the ratio of hoop to radial strain, was calculated by Eq. 1 [29]. The parameters of Eq. 1 were achieved by precisely measuring the internal and external diameter before and after the uniform plastic deformation. Table 1 records the mechanical
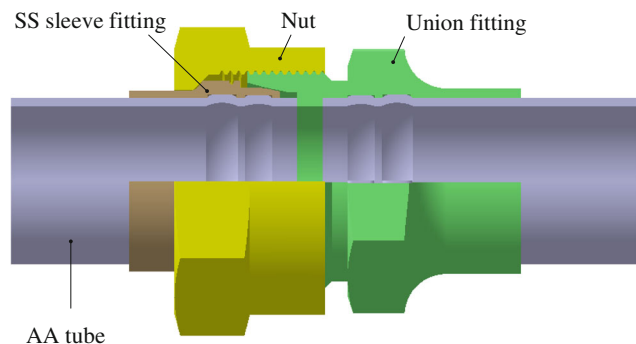

Fig. 1 A detachable joining method for connecting two separable end fittings

properties of the AA 6061-T4 tube.

$$r = \varepsilon_\theta/\varepsilon_t = \ln[(D_1 + d_1)/(D_0 + d_0)]/\ln(t_1/t_0) \qquad (1)$$

where ε_b is the radial strain; ε_t is the hoop strain; D_0 is the initial external diameter; D_1 is the external diameter when the strain is 15%; d_0 is the initial internal diameter; d_1 is the internal diameter when the strain is 15%; t_0 is the initial thickness; t_1 is the thickness when the strain is 15%.

The quadratic plastic yield criteria Hill48 is selected to describe the anisotropic plastic deformation behavior of the material as shown in Eq. 2 [30]. Using Eq. 3 [31], the parameter R_{11} in Abaqus/CAE, i.e., the yield stress ratio of radial and axial direction, could be calculated. The AA tube can be regarded as the isotropic hardening, and the Voce equation is adopted to characterize the work hardening of AA 6061-T4 tube. The fitting equation is shown in Eq. 4.

$$F\left(\sigma_y - \sigma_z\right) + G(\sigma_z - \sigma_x) + H\left(\sigma_x - \sigma_y\right) + 2L\tau_{yz}^2 + 2M\tau_{zx}^2$$
$$+ 2N\tau_{xy}^2$$
$$= \overline{\sigma}^2 \qquad (2)$$

$$r = H/G = \varepsilon_\theta/\varepsilon_r = 2(\sigma_t/\sigma_s)^2 - 1 = 2R_{11}^2 - 1 \qquad (3)$$

$$\sigma = 392.92 - 224.63 \exp(-10.88\varepsilon) \qquad (4)$$

2.2.2 PUE tube

PUE presents very complicated mechanical behavior that exceeds the linear elastic theory and contains large deformations, plastic and viscoelastic properties, nearly incompressible attributes, and stress softening [32], viz., the Mullins effect at the initial loading cycle [33]. These characteristics present complications in modeling the mechanical behaviors of PUE. Correspondingly, special experimentations including uniaxial tension, equal biaxial tension, and planar tension should be carried out to obtain the mechanical response [34]. The PUE tube used in this paper is 95A COURBHANE, and the geometry and dimensions are $\Phi17.6 \times t2.8$ mm. Since the PUE tube has no shear deformation in the EB process and the equal biaxial tension is equivalent to the uniaxial compression, the uniaxial tension and the uniaxial compression tests were conducted only in this paper. Hyperelastic material model, viz., three-order Ogden model, was adopted to fit the test data input into the material model in Abaqus/CAE and simulate the deformation behavior of the PUE tube. Ogden model is a constitutive model of phenomenological description based on the theory of continuum mechanics. This model proposes the strain energy function based on the principal stretches (λ_1, λ_2, λ_3) for incompressible materials that is assumed $\lambda_1\lambda_2\lambda_3 = 1$. The relation of the Ogden strain energy potential is given by Eq. 5 [35].

Fig. 2 Schematic presentation of fabricating a tubular joint by EB process.
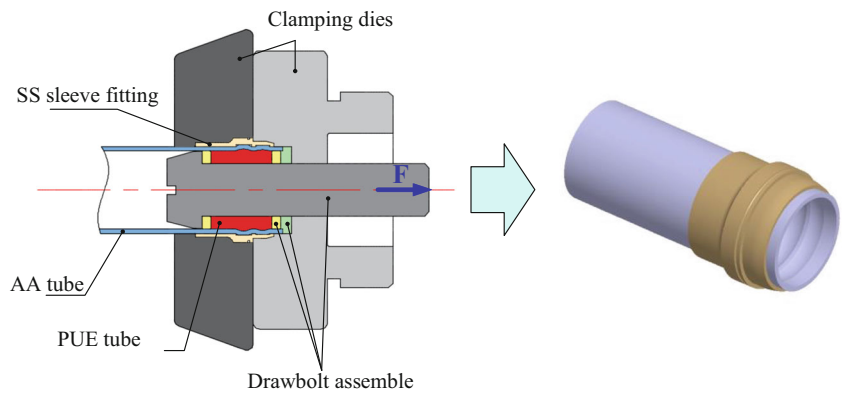
$$U = \sum_{i=1}^{N} 2u_i \left(\lambda_1^{\alpha_i} + \lambda_2^{\alpha_i} + \lambda_3^{\alpha_i} - 3 \right)/\alpha_i^2 + \sum_{i=1}^{N} (J_{el}-1)^{2i}/D_i \quad (5)$$

where $\lambda_i = J^{-1/3}\lambda_i$; $J = \lambda_1\lambda_2\lambda_3$; λ_i is the principal stretches; J is the Jacobean determinant; J_{el} is the elastic volume ratio.

According to the definitions of hyperelastic material model in Abaqus Analysis User's Guide [36], the nominal stress-strain curves are required to determine the stress-strain relationships of the PUE tube. The experimental data can be evaluated by the three-order Ogden model in Abaqus/CAE. Figure 4 shows the nominal stress-strain curves of this material in uniaxial tension and uniaxial compression, and it also shows the fitting results of the Ogden model with the experimental data. Due to the Mullins effect, the stress-strain curve of the fourth cycle was selected during the uniaxial compression test. The uniaxial compression test data was converted

into equal biaxial tensile test data for material modeling by means of Eq. 6~Eq. 11, and the equivalent biaxial stress-strain curve is illustrated in Fig. 4b.

Axial compressive strain:

$$\varepsilon_c = x/h_0 \quad (6)$$

Axial compressive stress:

$$\sigma_c = F_c/\pi R_0^2 \quad (7)$$

Radial biaxial tensile strain:

$$\varepsilon_b = R_x/R_0 = \left[\sqrt{R_0^2 h_0/(h_0-x)} - R_0 \right]/R_0$$

$$= \sqrt{h_0/(h_0-x)} - 1 \quad (8)$$

Radial biaxial tensile stress:

$$\sigma_b = F_t/2\pi R_0 h_0 \quad (9)$$

By using Eqs. (6), (7), (8), and (9), the following can be obtained:

$$\sigma_c = \sigma_b(1 + \varepsilon_b)^3 \quad (10)$$
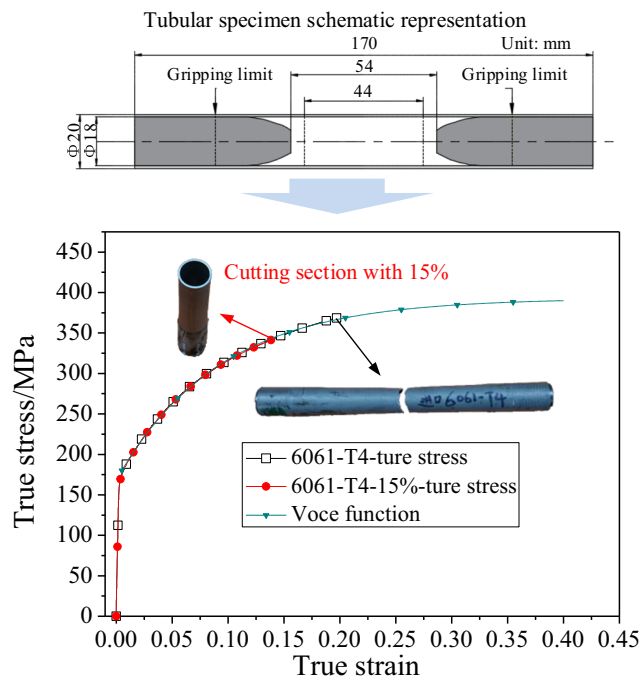
$$\varepsilon_c = 1/(1 + \varepsilon_b)^2 - 1 \quad (11)$$

2.2.3 SS 15-5PH sleeve fitting

15-5PH SS has the excellent comprehensive performance, such as higher strength and better elasticity. As for the EB processing, the SS sleeve fitting plays a critical role because of these special performances. Uniaxial tension test was

Fig. 3 The true stress-strain curve of AA 6061-T4 tube and fitting curves by the Voce hardening equation

Table 1 The mechanical properties of AA 6061-T4 tube

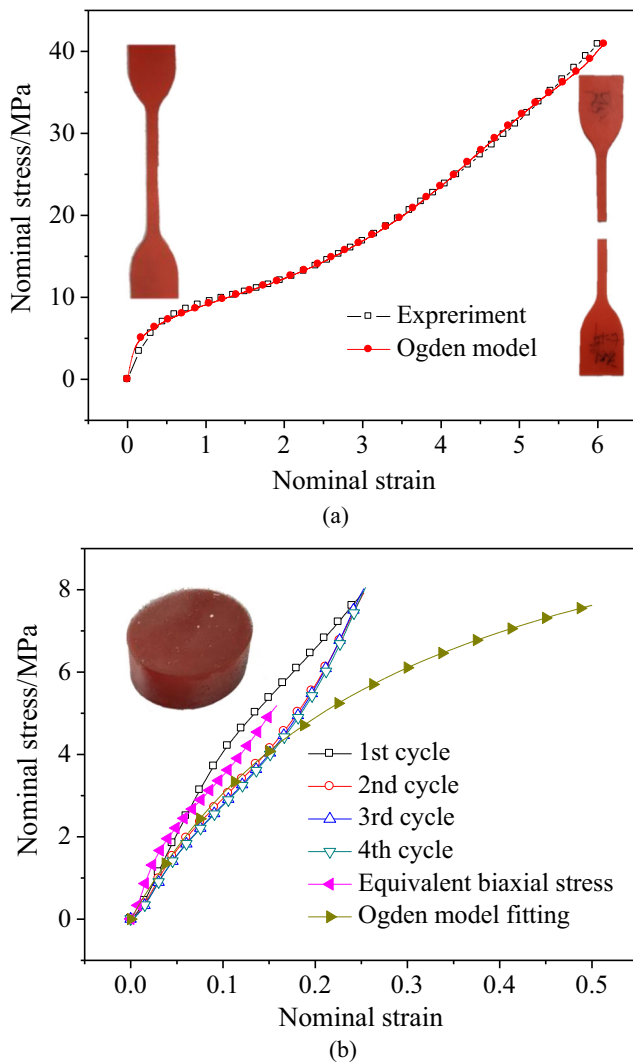| Material	E/GPa	δ /%	$\sigma_{0.2}$/ MPa	σ_b/ MPa	r
6061-T4	68.5	19.1	171.1	301.5	0.601

(a)

(b)

Fig. 4 Nominal stress-strain curve of the PUE material. **a** Uniaxial tension test. **b** Uniaxial compression test

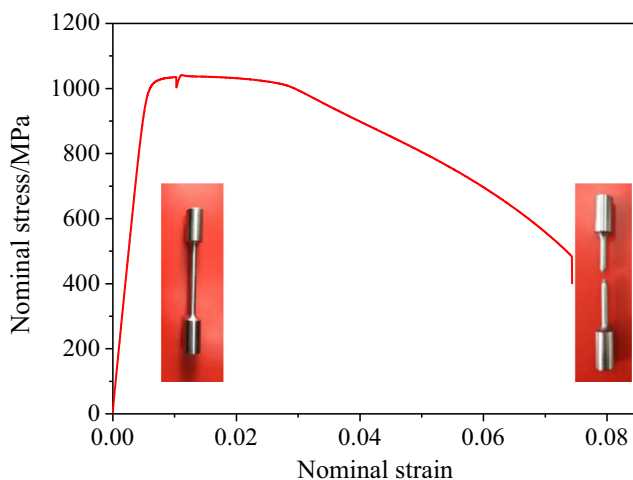**Fig. 5** The nominal stress-strain curve of SS 15-5PH

conducted to obtain the mechanical properties. Figure 5 shows the nominal stress-strain curve.

2.3 Experimental work plan

The experimental set-up and forming dies for EB joining tests are shown in Fig. 6a. By adjusting the pressure generated by the hydraulic pump of this set-up, the varied extrusion pressure can be obtained. Experimental case studies with different extrusion pressures in this paper are shown in Table 2. Figure 6b illustrates a formed test piece under extrusion pressure of 11 MPa.

Diameter measurement, destructive cutting, and optical microscope (OM) observation are used to validate and evaluate the forming quality. Diameter measurer, 1902 Mueller gauge, was applied to measure the bulging heights of the AA tube sandwiched in the grooves. In order to evaluate the forming quality visually, the tubular joining component was subjected to destructive cutting tests as shown in Fig. 7. And then, OM was used to observe the filling effect of the AA tube.

In order to verify the performance of the tubular joint fabricated by the EB processing, gaseous leakage (GL), proof pressure (PP), burst pressure (BP), and pull-out tests were carried out. The working pressure of the tubular joining fitting with diameter of 20 mm is prescribed as 4.31 MPa. The requirements for the above performance verification tests are shown in Table 3. As for the GL, PP, and BP tests, the working pressure is required, and the pull-out force is required for the pull-out test.

3 FE modeling of whole joining process

Whole process modeling of tubular joint forming by EB could be divided into two steps consisting of loading and unloading. The loading step is to simulate the EB process, while the unloading step is to model the springback process.

The geometry of all parts, the boundary conditions, and the loading conditions are all axisymmetric in the EB process, so an axisymmetric model could be used to simulate the whole process. This will greatly improve the computational efficiency. Furthermore, under the premise of ensuring the accuracy, the geometrical models in Fig. 2 are also simplified greatly (see Fig. 8a).

There are five parts in this model to be meshed as shown in Fig. 8b. Both the drawbolt and retaining ring adopt rigid element RAX2, a 2-node linear axisymmetric rigid link, to be discretized into 31 elements and 15 elements, respectively. The SS sleeve fitting and the AA tube both took advantage of deformable element CAX4R, a 4-node bilinear axisymmetric quadrilateral, reduced integration, and hourglass control element to achieve discretization. The total number of elements of the sleeve is 1007 and the tube is 2000. The PUE

Fig. 6 EB joining tests. **a** EB machine, forming dies, and their assembly model. **b** A formed test piece by EB under extrusion pressure of 11 MPa
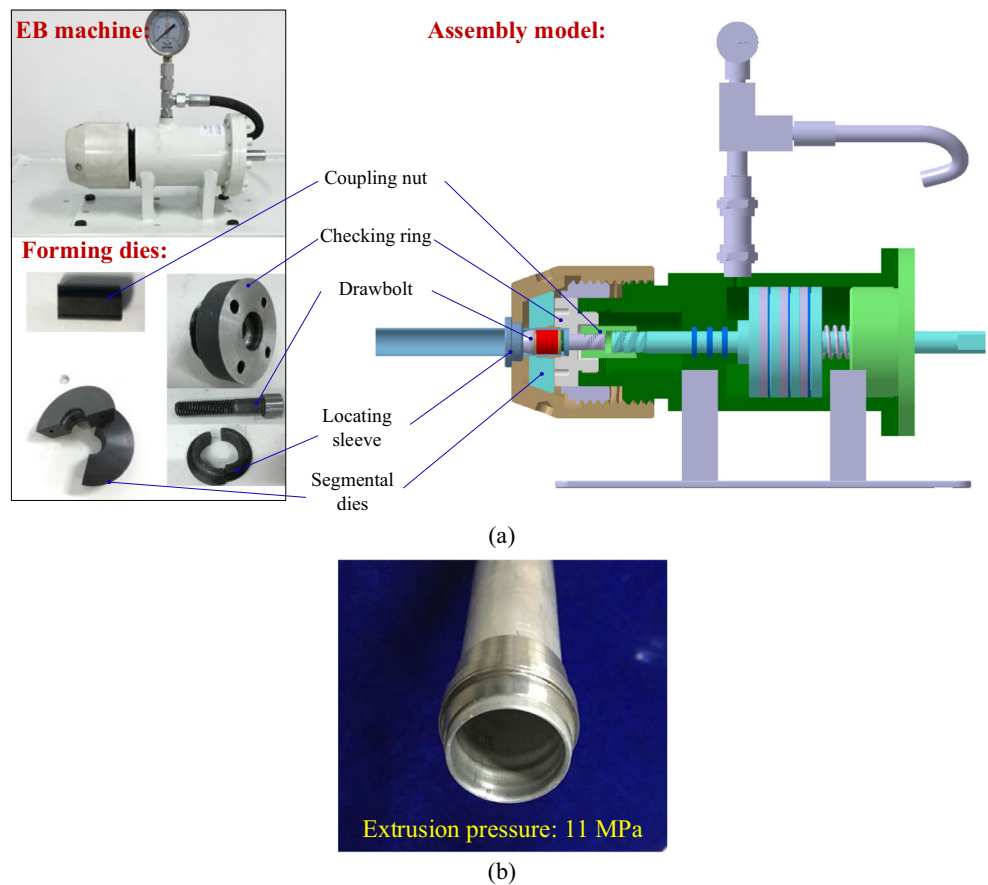
tube has different element types for the implicit and explicit algorithm. When the implicit algorithm was applied to the model analysis, CAX4RH, a 4-node bilinear axisymmetric quadrilateral, hybrid, constant pressure, reduced integration, and hourglass control element type, was utilized to the PUE tube, and the total element number was 1120. By contrast, the element type of the PUE tube will be identical with the sleeve and the tube if the explicit algorithm is adopted, and the element number remained unchanged.

The interactions in this model mainly includes the AA tube-SS sleeve fitting contacting, the PUE tube-AA tube contacting, the rigid dies-PUE tube contacting and the rigid dies-AA tube contacting. The sliding formulation chose finite sliding to character the interaction of surface-to-surface among all the parts. And the friction between the contact surfaces is calculated by the Coulomb friction model. In this model, the friction coefficient of the AA tube-sleeve fitting contacting is 0.15, the friction coefficient of the AA tube-PUE tube contacting is 0.08 with lubrication, the friction

coefficient of rigid dies-PUE tube contacting is 0.18, and the friction coefficient of rigid dies-AA tube contacting is 0.15.

As can be seen from Fig. 2, EB is a strictly multiple-tool constrained process, so it is essential to exert reasonable boundary conditions. In this model, displacement's amplitude control is applied to achieve boundary constrains and load exertion, so that the actual working conditions can be applied in the simulation process. All the 6 degrees of freedom of the sleeve fitting and the retaining ring are restrained in the whole process, while the tube is free. The drawbolt moves only with axial freedom to complete the loading and unloading process.

Based on the same material properties, contact conditions and boundary conditions, the explicit and the implicit algorithm in Abaqus/CAE were respectively adopted to simulate the EB process. With the appropriate ratio of kinetic energy to internal energy, the simulation result of the explicit algorithm is shown in Fig. 9. As can be seen from it, no plastic deformation occurs in the AA tube, while the implicit algorithm indicated the anticipant and normative result that the AA tube is bulged into the grooves of the sleeve fitting by the axially compressed PUE tube as shown in Fig. 10a. The most evident distinguish between the explicit and implicit models lies in the element type of the PUE tube that is CAX4R for the explicit while CAX4RH for the implicit. So as can be explained, the explicit algorithm is not suitable to simulate the precise

Table 2 Experimental work plan

Case	1	2	3	4	5
Extrusion pressure/MPa	10.0	10.5	11.0	11.5	12.0
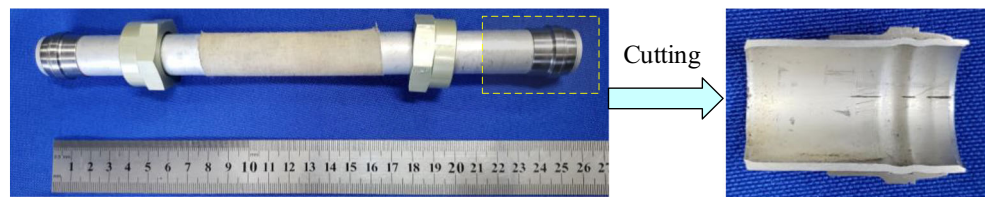
deformation behavior of the PUE tube, but hybrid formulation inhering in the implicit algorithm has obvious advantages over the explicit in coping with the highly constrained PUE. Hybrid elements can describe almost incompressible hyperelastic materials with initial Poisson's ratio greater than 0.495 (i.e., the ratio of K_0/μ_0 greater than 100) to avoid potential convergence problems. Additionally, in terms of computing time, the implicit algorithm is much shorter for the EB process than the explicit, and the time of the implicit algorithm is probably 5 min while the explicit is up to 3 h. Therefore, the implicit algorithm in Abaqus/Standard is applied into the whole process modeling.

Overall, the simulation for EB forming and springback of the tubular joints was carried out. Figure 10 illustrates the simulation results before and after springback when the extrusion depth is 2.45 mm.

4 Result and discussion

4.1 Influence of groove structure on pull-out strength and bonding strength

The influence of groove structure of sleeve fittings on forming quality is very crucial, and pull-out strength and bonding strength are two significant indexes to evaluate forming quality. Pull-out strength reflects the ability to resist the pressure on the end face of tubular profiles generated by working pressure of fluid in ducts, and it is assessed by pull-out force. Bonding strength indicates the ability to prevent the leakage, viz., deformation-induced sealing performance, and it is evaluated by the interference pressure, viz., contact shear stress between the AA tube and the SS sleeve fitting. According to the studies [12, 37], narrower and deeper rectangular grooves can lead to higher pull-out strength. However, this is only for form-fit joints without considering bond strength. As for the tubular

joint in this paper, it has the features of both interference-fit and form-fit. Thus, reasonable groove structure is particularly significant. In the following, taking pull-out strength and bonding strength into account, the groove structure of the sleeve fitting is designed and analyzed.
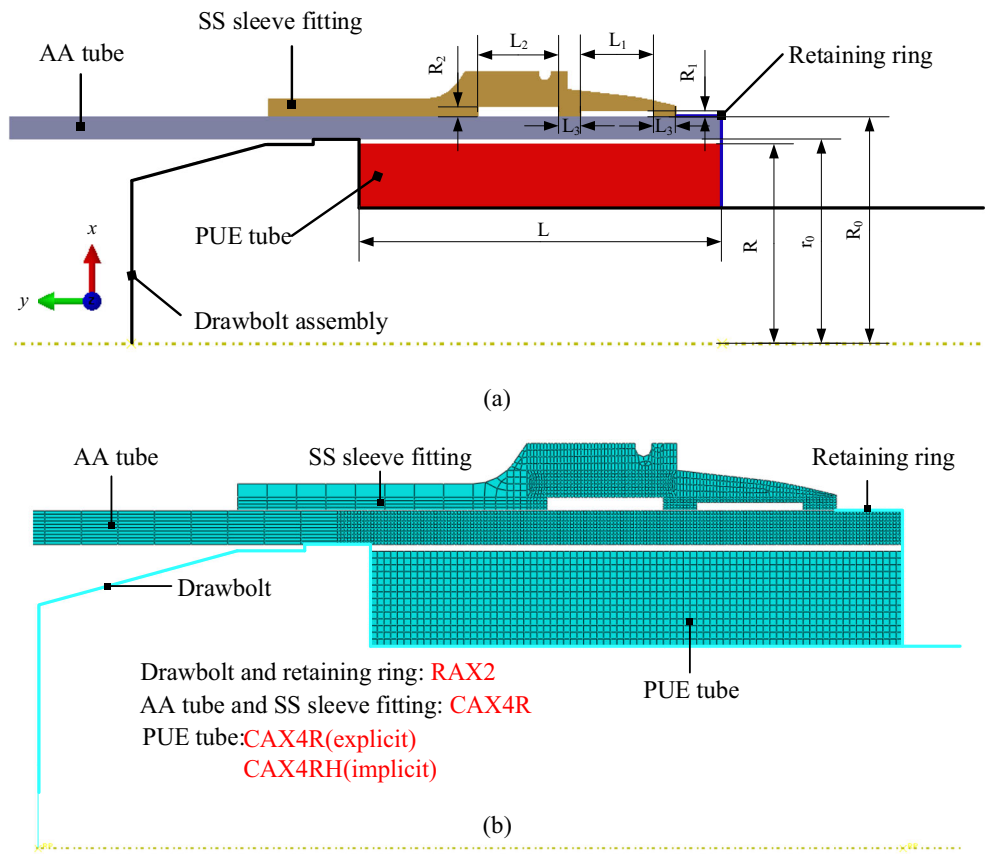
Figure 11 illustrates a cross-sectional view of a formed tubular joint with two rectangular grooves. Due to stress concentration and shearing at groove corners, there is certainly a limit for a groove, and the maximum depth of a groove is determined to be 0.4 mm. In addition, in views of multi-groove structure, different grooves have different limit depths for the EB processing. This is caused by internal friction of PUE and external friction with the other parts in the EB process, which leads to the inhomogeneous internal pressure against the inner wall of the AA tube along the axial direction. For the two grooves' structure, the distribution of the internal pressure is shown in Fig. 12. It is indicated that the bulge height of the AA tube in the two grooves will be varied therewith. Therefore, the distribution of groove depth should also be corresponding to the distribution of the bulge height of the AA tube, so that the tube wall can lie against the groove bases at the same time, and finally interference-fit connection can be formed simultaneously between the AA tube and the groove bases. Figure 13 shows the relationship between the bulge height of the AA tube and the extrusion depth of the drawbolt. It can be obtained from this figure that the back groove depth R_2 (see Fig. 8a) is 0.15 mm larger than the front groove depth R_1. So, the two grooves' depth R_1 and R_2 can be designed to be 0.25 mm and 0.4 mm, respectively. Meanwhile, in order to avoid stress concentration at the shape transition of the sleeve fitting in the bulging process, the two grooves' width L_1 and L_2 (see Fig. 8a) are designed to be 3.2 mm and 3.3 mm respectively, and the groove location size L_3 (see Fig. 8a) is 1 mm.

According to the above groove structure design, the sleeve fittings with single groove and double grooves are used to simulate the whole process of EB joining. On this basis, the bonding strength of single groove and double grooves is compared after springback of all parts as shown in Fig. 14. As can be seen from this figure, the bonding strength with double grooves is higher than single groove near the sharp edges of the groove. There are more positions to generate interference-fit connection, for instance, at the two sharp edges of the front groove and at the middle of the two groove bases. Therefore,

Table 3 The requirements for the performance verification tests

Case	Quantity and number	Requirements
GL	No. 1–6	4.31 MPa
PP	No. 1–12	8.62 MPa
BP	No. 7–12	17.24 MPa
Pull-out	No. 13–14	5.41 kN

Fig. 8 Simplified geometric model and corresponding finite element mesh of the EB process. **a** Axisymmetric model after simplification. **b** Element types of different parts

(a)

Drawbolt and retaining ring: RAX2
AA tube and SS sleeve fitting: CAX4R
PUE tube: CAX4R(explicit)
                 CAX4RH(implicit)

(b)

the double grooves structure is more resistant to working pressure to prevent leakage.

And then, the simulation for the pull-out test is carried out to compare the pull-out strength of single groove and double grooves. Figure 15 illustrates the distribution of reaction force, viz., pull-out force, of these two structures in the pull-out process. From this figure, it can be obtained that the maximum pull-out force of double grooves is greater than that of single groove, and the double grooves structure is more resistant to damage under the same tensile rate. Referring to the requirements of pull-out test in Section 2.3, the double grooves structure is completely qualified. Accordingly, there is no need to consider more groove structures, which will increase the processing cost.

4.2 Precise control of forming quality of tubular joints fabricated by EB

Base on the above double grooves structure, this section further discusses the precise control of forming quality of the tubular joints. In views of the EB processing, extrusion pressure is a key parameter for fabricating the tubular joints with excellent bonding strength and pull-out strength, and then the bulging heights of the tube sandwiched in the two grooves of the sleeve fitting are significant parameters to evaluate the bonding strength and pull-out strength indirectly. Thus, accurate and reasonable extrusion pressure and tube bulging heights are the key to precise control of forming quality. These two factors can be determined by theoretical analysis
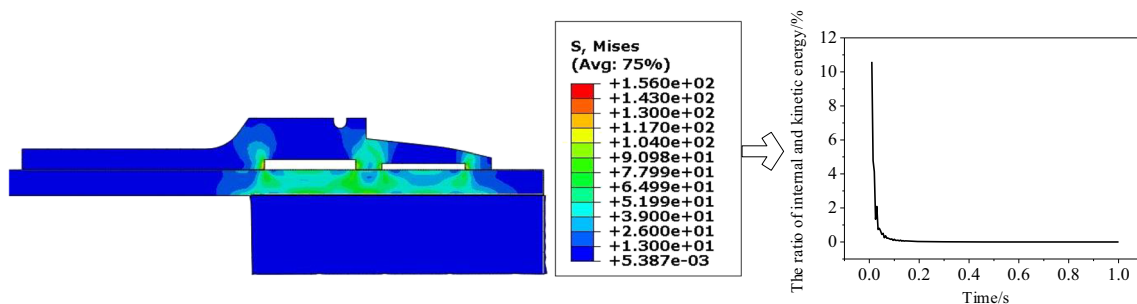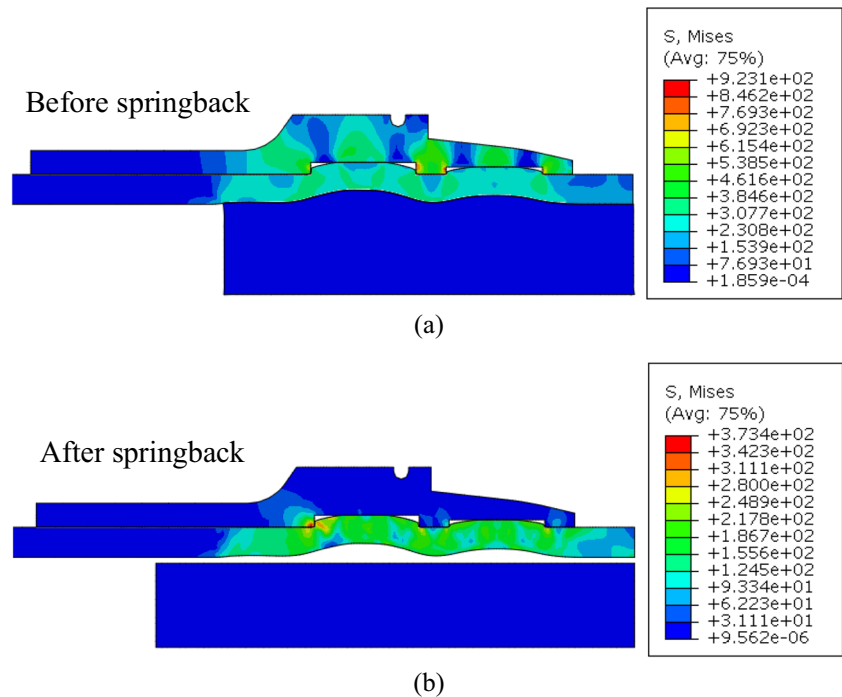

Fig. 9 The simulation results of the EB process with Abaqus/Explicit

Fig. 10 Simulation results under the extrusion depth of 2.45 mm. **a** Before springback. **b** After springback

(a)

(b)

and numerical simulation. The details are shown in the following steps:

1. Based on the bulk incompressibility of the materials, the theoretical limit value y of the extrusion depth of the drawbolt can be calculated by Eqs. (12), (13), and (14), approximately equal to 2.5 mm. This value provides a reference of the extrusion depth for FE simulation.

$$y = y_1 + y_2 \tag{12}$$

$$y_1 = \pi\left(r_0{}^2 - R^2\right)L / \pi r_0{}^2 \tag{13}$$

$$y_2 = \pi\left(R_1{}^2 - R_0{}^2\right)L_1 + \pi\left(R_2{}^2 - R_0{}^2\right)L_2 / \pi r_0{}^2 \tag{14}$$

where y is the theoretical limit value of extrusion depth of the drawbolt; y_1 is the extrusion depth of the drawbolt when the PUE tube is just in full contact with the AA tube; y_2 is the extrusion depth of the drawbolt when it is assumed that the AA tube is bulged to fill the grooves without any cavities; the other parameters are illustrated in Fig. 8a.

2. Combined with this theoretical limit value y and the simulation for EB processing, the ultimate extrusion depth of the drawbolt, 2.45 mm, is obtained.

3. According to the ultimate extrusion depth and the reaction force of the reference point of the drawbolt, the extrusion forming force F_d of the drawbolt can be obtained by displacement amplitude control as shown in Fig. 16. As can be seen from this figure, stage 1 is that the drawbolt axially presses the PUE tube until it contacts with the AA tube; stage 2 is that the PUE tube produces inner pressure to make the tube bulge locally and the AA tube is gradually squeezed into the grooves of the SS sleeve fitting; stage 3 is that the AA tube continues to fill the grooves when the outer wall of AA tube contacts with the bottom of the SS sleeve fitting's grooves. It can be inferred that stage 3 is an essential one to obtain a sealing ring between the AA tube and the SS sleeve fitting. Therefore, it is crucial to load to stage 3, which directly determines the deformation-induced sealing performance of the tubular joints.

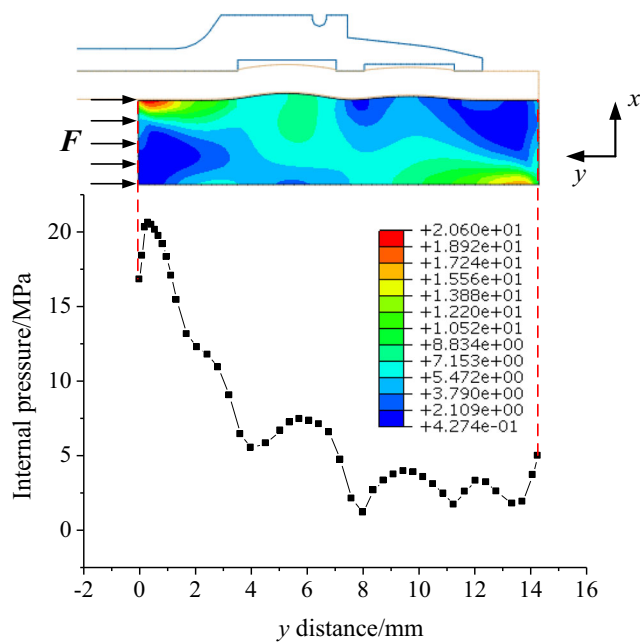**Fig. 11** A cross-sectional view of a formed tubular joint with two rectangular grooves
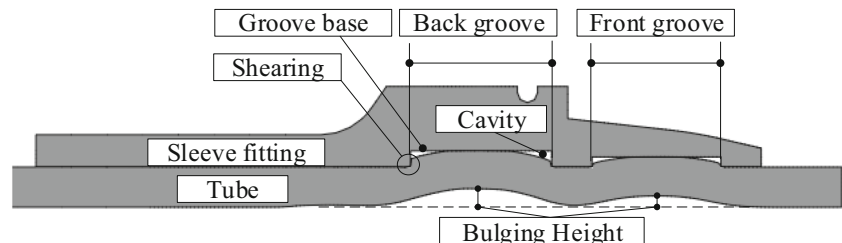
Fig. 12 The distribution of the internal pressure on the inner wall of the AA tube

4. The initial F_d range, i.e., the data in stage 3, of the drawbolt can be confirmed through analyzing the curve in Fig. 16. So, the F_d range is preliminarily ascertained to be 21.857~59.7 kN. Correspondingly, the extrusion depth range is also determined to be 2.09~2.45 mm. Due to the radial springback of the tube and the sleeve fitting in the same direction after the EB forming, it can be inferred that the minimum in this range is not able to produce enough interference stresses to form a seal. The above range needs to be further determined. For this purpose, the relationship between the bonding strength and the extrusion depth is revealed, as illustrated in Fig. 17. This can explain why the sealing performance is unstable. When high pressure is applied in the tube, greater interference stress
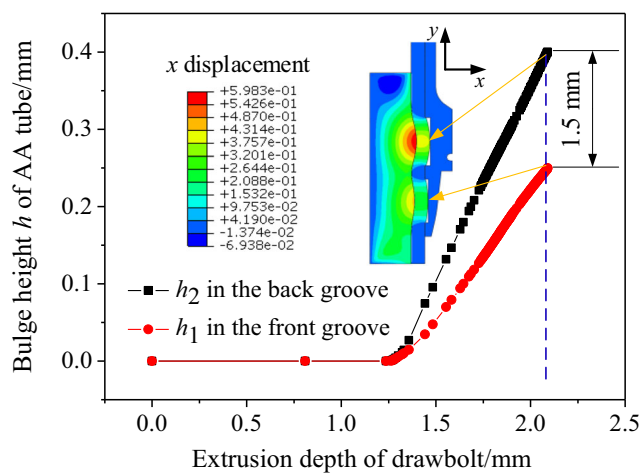

Fig. 13 The relationship between the bulge height of AA tube and the extrusion depth of the drawbolt in the EB forming process
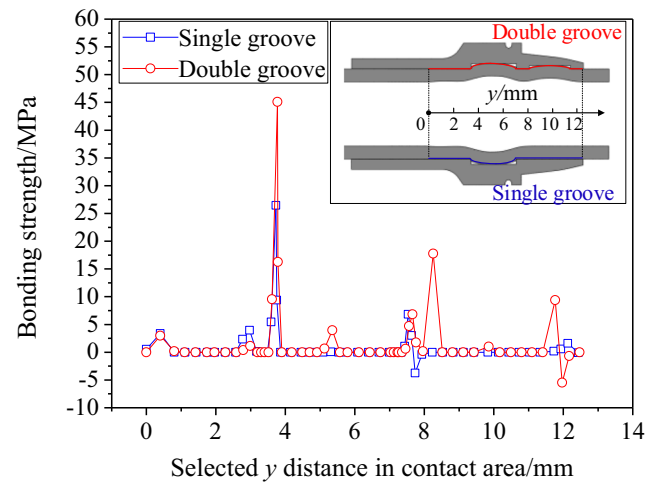

Fig. 14 Comparison of bonding strength after joining between two different sleeve fittings with a single groove and double grooves

will be produced between the tube and the sleeve fitting, and vice versa. In addition, it can be found from Fig. 14 that the contact points between the groove edge of the sleeve fitting and the tube, viz., location 1, 3, 4, and 6 in Fig. 17, have greater bonding strengths, and there are also interference stresses in the contact points between the middle of the groove bases and the tube, viz., location 2 and 5 in Fig. 17. As can be seen from Fig. 17, there is maximum bonding strength at location 6. It can be explained that the tube at this location is subjected to the greater internal pressure than the other locations (see Fig. 12). So, there is maximum elastic deformation on this sharp edge of the sleeve fitting, generating the maximum interference stress after the springback of the two parts. This location can meet the requirements of the performance tests in Table 3. In addition, when the extrusion depth is greater than 2.35 mm, there is slightly small bonding strength at location 2 and 5, so enough
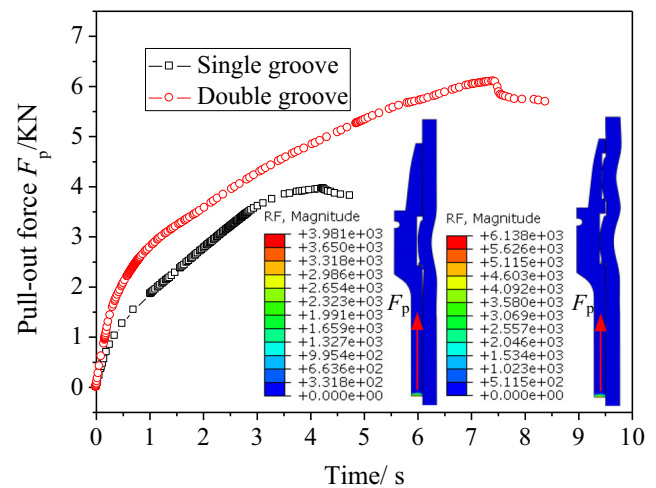

Fig. 15 Comparison of pull-out force F_p between two different sleeve fittings with a between single groove and double grooves

interference stress cannot be generated to resist leakage at these two locations. And the maximum bonding strength at location 4, 6.73 MPa, is also low, so that it cannot satisfy the demand of the PP test. Location 1 is the first barrier to resist the working pressure, but the maximum at this position is 10.7 MPa which cannot meet the requirement of BP test. Meanwhile, location 3 needs to play its role, so it is essential that the extrusion depth is greater than 2.3 mm. Taking the above-mentioned into account, for more resistance barriers and greater bonding strength, the extrusion depth of the drawbolt is ultimately determined to be 2.3~2.45 mm. According to Fig. 16, it can be obtained that the F_d range is 48.6~59.7 kN.

5. According to Eq. 15, the range of extrusion pressure P_f for the EB process is 10.0~12.3 MPa.

$$P_f = F_d / S_p \qquad (15)$$

where S_p is the piston area, 4825.5 mm^2.

6. Figure 18 illustrates the relationship between the tube bulging height H_b and the extrusion depth of the drawbolt. As can be seen from this figure, it can be obtained that the reasonable range of the tube bulging heights H_b sandwiched in the two grooves after springback of all the deformation parts. The ranges of H_{b1} and H_{b2} are 0.435~0.460 mm and 0.265~0.280 mm, respectively.

4.3 Experimental verification

Based on the above extrusion forming pressure calculated by the FE model, the tubular joints were fabricated by using the set-up in Section 2.3. The extrusion forming pressures in Table 2 were applied in the EB joining experiments by
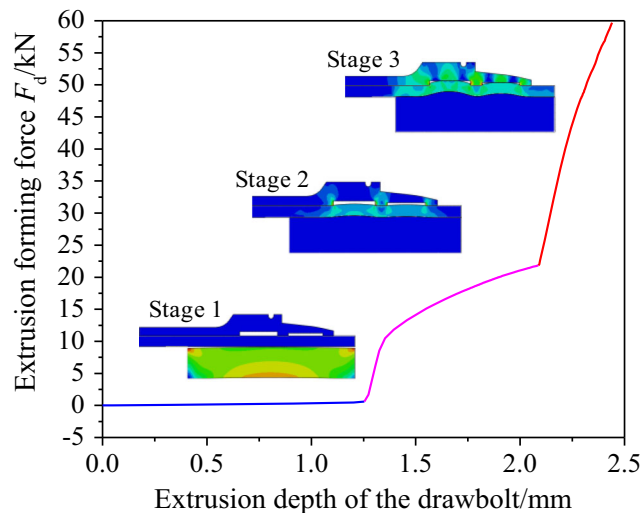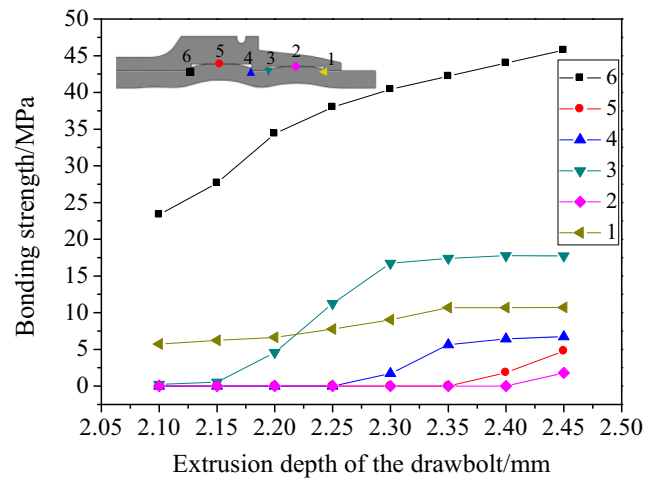
Fig. 17 The relationship between the bonding strength and the extrusion depth of the drawbolt at six different locations

controlling the pressure displayed on the oil gauge. Then, destructive cutting experiments were used in the fabricated joining components. Figure 19a illustrates the comparison of the tube bulging heights between the simulation result and the experiment result under the extrusion pressure of 10 MPa. By means of OM, the experiment result was the patched longitudinal section of the joint. It can be inferred that the filling effects of simulation and experiment are in good agreement with each other. Furthermore, comparison of the tube bulge heights sandwiched in the two grooves between simulation and experiment under different pressures are shown in Fig. 19b. It can be found that the process parameters calculated by the FE model are accurate and reliable.

In views of the other performance verification tests, 14 tubular joining components were fabricated by EB joining process with the above parameter calculated by the FE model. These components were numbered "No. 1~14," and the quantity required for each test is shown in Table 3. In the GL test, No. 1~6 components were immersed in water, and they are
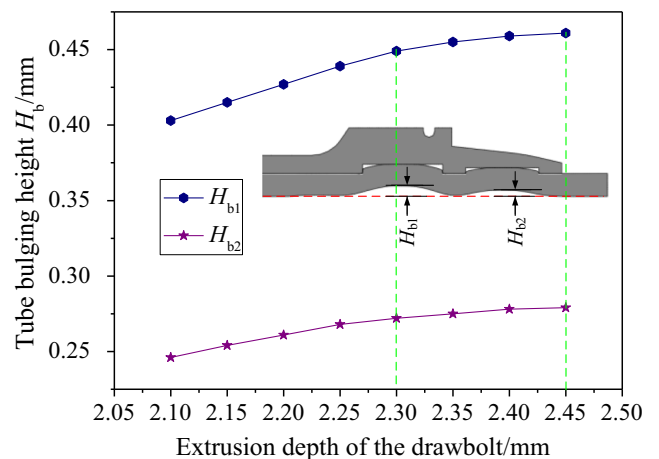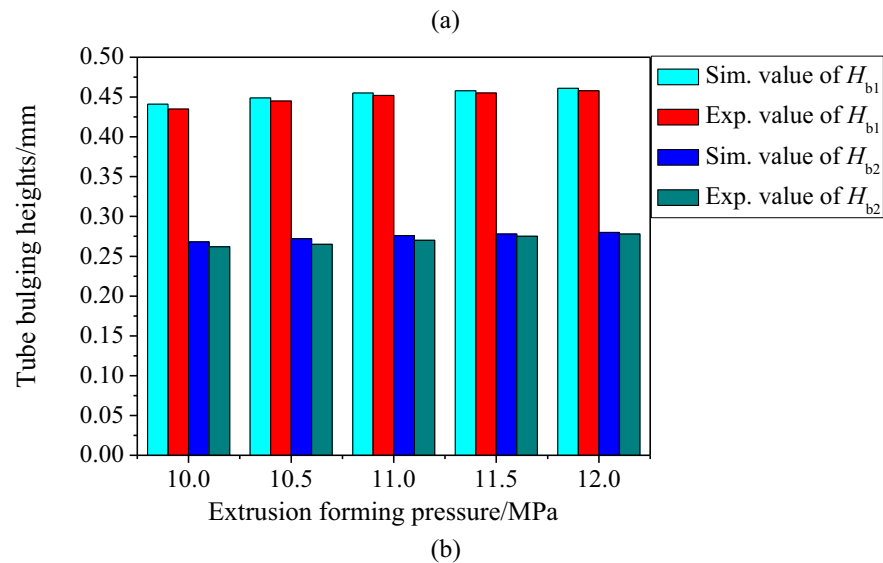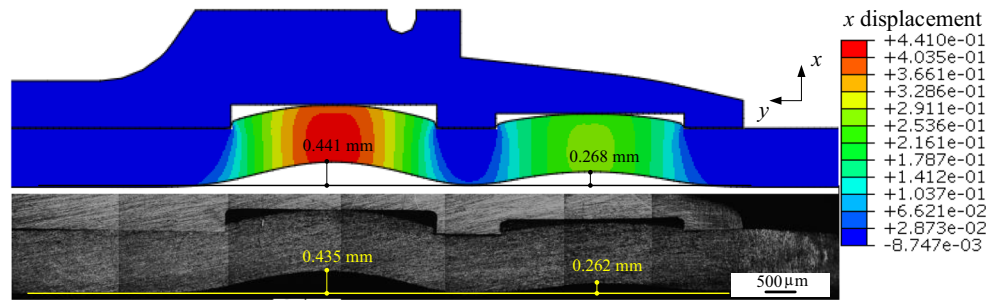
Fig. 16 Evolution of extrusion forming force F_d with extrusion depth of the drawbolt

Fig. 18 The relationship between the tube bulging height H_b and the extrusion depth of the drawbolt

Fig. 19 Comparison of the tube bulge heights between simulation and experiment. **a** Under the extrusion forming pressure of 10 MPa. **b** Under different extrusion forming pressures

(a)

(b)

filled with air to the work pressure and maintain the pressure for 5 min. As a result, no bubbles came out in these components. In the PP test, all the components were pressurized twice the work pressure with the pressure rise rate of 30 ± 7.5 MPa/min for 5 min, and then they had no leakage/deformation. No. 7~12 components also had no leakage and break during pressurization to 4 times the working pressure in the BP test. As for No. 13~14 components, when these two components were loaded to 5.41 kN, the sleeve fitting did not slip off the AA tube and it was not cracked. Instead, when the sleeve fitting slipped off the AA tube, the ultimate pull-out forces were 6.25 kN and 6.05 kN, respectively. Overall, the sealing performance of the tubular joining components fabricated by the EB process is reliable.

5 Conclusion

In this paper, thin-walled AA 6061-T4 tubular joint forming based on EB was investigated experimentally and numerically. The problem of unstable seals has been improved by precisely controlling bonding strength and pull-out strength, and the service performance has been verified based on the established experimental set-up and forming dies for EB joining. The main conclusions can be drawn as follows:

1. Based on the characterization of mechanical properties of AA6061-T4 tube, PUE tube, and 15-5PH SS sleeve fitting, an anisotropic material model based on the quadratic plastic yield criteria Hill48 was established for AA6061-T4 tube; a hyperelastic material model based on three-order Ogden model was adopted for PUE tube; in addition, an isotropic material model was used for 15-5PH SS.

2. Axisymmetric FE models of the whole joining process, including EB forming and unloading, were established and experimentally validated. Compared with the explicit algorithm, the implicit algorithm was selected to model the EB process. The influence of groove structure on the forming quality was analyzed. It was found that the structure of double grooves with reasonable structural dimensions could obtain stronger bonding strength and pull-out strength. Furthermore, the proper extrusion pressure range, 10.0~12.3 MPa, and ranges of tube bulging heights H_{b1} and H_{b2}, 0.435~0.460 mm and 0.265~0.280 mm, were also obtained, and thus the precise control of forming quality can be achieved.

3. By measuring the tube bulging heights sandwiched in the grooves and observing the longitudinal profile morphology by means of OM, the effectiveness of the FE model were validated. Moreover, the sealing performance of the tubular joining components were verified through the GL, PP, and BP tests. Therefore, tubular components with reliable sealing performance can be fabricated by using the process parameters calculated by the FE model.

References

1. Li H, Fu MW (2019) Deformation-based processing of materials. Elsevier. https://doi.org/10.1016/C2017-0-01559-8

2. Yang H, Li H, Zhang Z, Zhan M, Liu J, Li G (2012) Advances and trends on tube bending forming technologies. Chin J Aeronaut 25(1):1–12. https://doi.org/10.1016/s1000-9361(11)60356-7

3. Wanhill R, Ashok B (2017) Shape memory alloys (SMAs) for aerospace applications. Aerospace Materials and Material Technologies. Springer, In, pp 467–481

4. Yang H, Li H, Ma J, Wei D, Chen J, Fu MW (2019) Temperature dependent evolution of anisotropy and asymmetry of α-Ti in thermomechanical working: Characterization and modeling. Int J Plast 2019:102650 (In press). https://doi.org/10.1016/j.ijplas.2019.102650

5. Li H, Wei D, Zhang HQ, Yang H, Zhang D, Li GJ (2019) Tooling design–related spatial deformation behaviors and crystallographic texture evolution of high-strength Ti-3Al-2.5 V tube in cold pilgering. Int J Adv Manuf Technol 104(5–8):2851–2862. https://doi.org/10.1007/s00170-019-04151-w

6. Wang HP, Lü P, Cai X, Zhai B, Zhao JF, Wei B (2020) Rapid solidification kinetics and mechanical property characteristics of Ni–Zr eutectic alloys processed under electromagnetic levitation state. Mater Sci Eng A 772:138660. https://doi.org/10.1016/j.msea.2019.138660

7. Feng ZY, Li H, Yang JC, Huang H, Li GJ, Huang D (2018) Macro-meso scale modeling and simulation of surface roughening: Aluminum alloy tube bending. Int J Mech Sci 144:696–707. https://doi.org/10.1016/j.ijmecsci.2018.06.032

8. K-i M, Bay N, Fratini L, Micari F, Tekkaya AE (2013) Joining by plastic deformation. CIRP Ann 62(2):673–694. https://doi.org/10.1016/j.cirp.2013.05.004

9. Groche P, Wohletz S, Brenneis M, Pabst C, Resch F (2014) Joining by forming—a review on joint mechanisms, applications and future trends. J Mater Process Technol 214(10):1972–1994. https://doi.org/10.1016/j.jmatprotec.2013.12.022

10. Henriksen J, Nordhagen HO, Hoang HN, Hansen MR, Thrane FC (2015) Numerical and experimental verification of new method for connecting pipe to flange by cold forming. J Mater Process Technol 220:215–223. https://doi.org/10.1016/j.jmatprotec.2015.01.018

11. Przybylski W, Wojciechowski J, Klaus A, Marré M, Kleiner M (2006) Manufacturing of resistant joints by rolling for light tubular structures. Int J Adv Manuf Technol 35(9–10):924–934. https://doi.org/10.1007/s00170-006-0775-0

12. Weddeling C, Woodward ST, Marré M, Nellesen J, Psyk V, Tekkaya AE, Tillmann W (2011) Influence of groove characteristics on strength of form-fit joints. J Mater Process Technol 211(5):925–935. https://doi.org/10.1016/j.jmatprotec.2010.08.004

13. Gies S, Weddeling C, Marré M, Kwiatkowski L, Tekkaya AE (2012) Analytic prediction of the process parameters for form-fit joining by die-less hydroforming. Key Eng Mater 504-506:393–398. https://doi.org/10.4028/www.scientific.net/KEM.504-506.393

14. Zhang Q, Jin K, Mu D (2014) Tube/tube joining technology by using rotary swaging forming method. J Mater Process Technol 214(10):2085–2094. https://doi.org/10.1016/j.jmatprotec.2014.02.002

15. Yang JC, Li H, Huang D, Li GJ (2020) Deformation-based joining for high-strength Ti-3Al-2.5V tubular fittings based on internal roller swaging. Int J Mech Sci 171:105376. https://doi.org/10.1016/j.ijmecsci.2019.105367

16. Merklein M, Allwood JM, Behrens BA, Brosius A, Hagenah H, Kuzman K, Mori K, Tekkaya AE, Weckenmann A (2012) Bulk forming of sheet metal. CIRP Ann 61(2):725–745. https://doi.org/10.1016/j.cirp.2012.05.007

17. Alves LM, Martins PAF (2012) Tube branching by asymmetric compression beading. J Mater Process Technol 212(5):1200–1208. https://doi.org/10.1016/j.jmatprotec.2012.01.004

18. Zhang Q, Zhang Y, Cao M, Ben N, Ma X, Ma H (2016) Joining process for copper and aluminum tubes by rotary swaging method. Int J Adv Manuf Technol 89(1–4):163–173. https://doi.org/10.1007/s00170-016-8994-5

19. Alves LM, Gameiro J, Silva CMA, Martins PAF (2017) Sheet-bulk forming of tubes for joining applications. J Mater Process Technol 240:154–161. https://doi.org/10.1016/j.jmatprotec.2016.09.021

20. Alves LM, Afonso RM, Silva CMA, Martins PAF (2018) Joining tubes to sheets by boss forming and upsetting. J Mater Process Technol 252:773–781. https://doi.org/10.1016/j.jmatprotec.2017.10.047

21. Alves LM, Silva CMA, Martins PAF (2014) End-to-end joining of tubes by plastic instability. J Mater Process Technol 214(9):1954–1961. https://doi.org/10.1016/j.jmatprotec.2014.04.011

22. Yu H, Li J, He Z (2018) Formability assessment of plastic joining by compression instability for thin-walled tubes. Int J Adv Manuf Technol 97(9–12):3423–3430. https://doi.org/10.1007/s00170-018-2128-1

23. Alves LM, Silva CMA, Martins PAF (2017) Joining of tubes by internal mechanical locking. J Mater Process Technol 242:196–204. https://doi.org/10.1016/j.jmatprotec.2016.11.037

24. Thiruvarudchelvan S (2002) The potential role of flexible tools in metal forming. J Mater Process Technol 122(2–3):293–300

25. Girard AC, Grenier YJ, Mac Donald BJ (2006) Numerical simulation of axisymmetric tube bulging using a urethane rod. J Mater Process Technol 172(3):346–355. https://doi.org/10.1016/j.jmatprotec.2005.10.012

26. Ramezani M, Ripin ZM, Ahmad R (2009) Computer aided modelling of friction in rubber-pad forming process. J Mater Process Technol 209(10):4925–4934. https://doi.org/10.1016/j.jmatprotec.2009.01.015

27. Koubaa S, Belhassen L, Wali M, Dammak F (2017) Numerical investigation of the forming capability of bulge process by using rubber as a forming medium. Int J Adv Manuf Technol 92(5–8):1839–1848. https://doi.org/10.1007/s00170-017-0278-1

28. Belhassen L, Koubaa S, Wali M, Dammak F (2017) Anisotropic effects in the compression beading of aluminum thin-walled tubes with rubber. Thin-Walled Struct 119:902–910. https://doi.org/10.1016/j.tws.2017.08.010

29. Li H, Yang H, Lu RD, Fu MW (2016) Coupled modeling of anisotropy variation and damage evolution for high strength steel tubular materials. Int J Mech Sci 105:41–57. https://doi.org/10.1016/j.ijmecsci.2015.10.017

30. Hill R (1948) A theory of the yielding and plastic flow of anisotropic metals. Proc R Soc Lond A 193(1033):281–297

31. Hill R (1998) The mathematical theory of plasticity, vol 11. Oxford university press
32. Hepburn C (2012) Polyurethane elastomers. **Springer Science & Business Media**,
33. Diani J, Fayolle B, Gilormini P (2009) A review on the Mullins effect. Eur Polym J 45(3):601–612. https://doi.org/10.1016/j.eurpolymj.2008.11.017
34. Sasso M, Palmieri G, Chiappini G, Amodio D (2008) Characterization of hyperelastic rubber-like materials by biaxial and uniaxial stretching tests based on optical methods. Polym Test 27(8):995–1004. https://doi.org/10.1016/j.polymertesting.2008.09.001
35. Ogden RW (1972) Large deformation isotropic elasticity–on the correlation of theory and experiment for incompressible rubberlike solids. Proc R Soc Lond A 326(1567):565–584
36. Systèmes D (2014) Abaqus analysis user's guide. Solid (Continuum) Elements 6
37. Park Y-B, Kim H-Y, Oh S-I (2005) Design of axial/torque joint made by electromagnetic forming. Thin-Walled Struct 43(5):826–844. https://doi.org/10.1016/j.tws.2004.10.009

Publisher's note Springer Nature remains neutral with regard to jurisdictional claims in published maps and institutional affiliations.